

UCSF

UC San Francisco Previously Published Works

Title

Patient-derived tumor explant models of tumor immune microenvironment reveal distinct and reproducible immunotherapy responses.

Permalink

<https://escholarship.org/uc/item/0k9264xf>

Journal

Oncolmmunology, 14(1)

Authors

Turpin, Rita
Peltonen, Karita
Rannikko, Jenna
[et al.](#)

Publication Date

2025-12-01

DOI

10.1080/2162402X.2025.2466305

Peer reviewed

Patient-derived tumor explant models of tumor immune microenvironment reveal distinct and reproducible immunotherapy responses

Rita Turpin^{a,b*}, Karita Peltonen^{c,d,e*}, Jenna H. Rannikko^b, Ruixian Liu^a, Anita N. Kumari^{c,d}, Daniel Nicorici^a, Moon Hee Lee^{c,d}, Minna Mutka^f, Panu E. Kovanen^f, Laura Niinikoski^g, Tuomo Meretoja^g, Johanna Mattson^h, Petrus Järvinenⁱ, Kanerva Lahdensuoⁱ, Riikka Järvinenⁱ, Sara Tornbergⁱ, Tuomas Mirtti^j, Pia Boström^k, Ilkka Koskivuo^l, Anil Thotakura^m, Jeroen Pouwels^a, Maija Hollmén^{b**,}, Satu Mustjoki^{c,d,e**,} and Juha Klefström^l 

^aCancer Cell Circuitry Laboratory, Translational Cancer Medicine, Medical Faculty, University of Helsinki, Helsinki, Finland; ^bMediCity Research Laboratory and INFLAMES Flagship, University of Turku, Turku, Finland; ^cHematology Research Unit Helsinki, University of Helsinki and Helsinki University Hospital Comprehensive Cancer Center, Helsinki, Finland; ^dTranslational Immunology Research Program, University of Helsinki, Helsinki, Finland; ^eiCAN Digital Precision Cancer Medicine Flagship, University of Helsinki and Helsinki University Hospital Comprehensive Cancer Center, Helsinki, Finland; ^fDepartment of Pathology, HUSLAB and Haartman Institute, Helsinki University Central Hospital and University of Helsinki, Helsinki, Finland; ^gDivision of Breast Surgery, Comprehensive Cancer Center, Helsinki University Hospital and University of Helsinki, Helsinki, Finland; ^hComprehensive Cancer Center, Helsinki University Hospital and University of Helsinki, Helsinki, Finland; ⁱAbdominal Center, Urology, Helsinki University and Helsinki University Hospital, Helsinki, Finland; ^jDepartment of Pathology, Helsinki University Hospital and Research Program in Systems Oncology, University of Helsinki, Helsinki, Finland; ^kDepartment of Pathology, Turku University Hospital, Turku, Finland; ^lDepartment of Digestive Surgery and Urology, Turku University Hospital and University of Turku, Turku, Finland; ^mImmuno-Oncology, Oncology Research, Orion Corporation, Turku, Finland; ⁿFinnish Cancer Institute, Helsinki, Finland; ^oFICAN South, Helsinki University Hospital, Helsinki, Finland; ^pDepartment of Cell & Tissue Biology, University of California, San Francisco, USA

ABSTRACT

Tumor-resident immune cells play a crucial role in eliciting anti-tumor immunity and immunomodulatory drug responses, yet these functions have been difficult to study without tractable models of the tumor immune microenvironment (TIME). Patient-derived *ex vivo* models contain authentic resident immune cells and therefore, could provide new mechanistic insights into how the TIME responds to tumor or immune cell-directed therapies. Here, we assessed the reproducibility and robustness of immunomodulatory drug responses across two different *ex vivo* models of breast cancer TIME and one of renal cell carcinoma. These independently developed TIME models were treated with a panel of clinically relevant immunomodulators, revealing remarkably similar changes in gene expression and cytokine profiles among the three models in response to T cell activation and STING-agonism, while still preserving individual patient-specific response patterns. Moreover, we found two common core signatures of adaptive or innate immune responses present across all three models and both types of cancer, potentially serving as benchmarks for drug-induced immune activation in *ex vivo* models of the TIME. The robust reproducibility of immunomodulatory drug responses observed across diverse *ex vivo* models of the TIME underscores the significance of human patient-derived models in elucidating the complexities of anti-tumor immunity and therapeutic interventions.

ARTICLE HISTORY

Received 25 October 2024
Revised 4 February 2025
Accepted 7 February 2025

KEYWORDS

Breast cancer; *ex vivo* model; immune checkpoint; IO-treatment; patient-derived explants; renal cell carcinoma; tumor immune microenvironment

Introduction

The field of immuno-oncology has revolutionized cancer care. Nevertheless, the effectiveness of immunotherapies on solid tumors has been notably modest, a phenomenon largely attributed to the complex interplay between tumor cells and immune-modulating factors within the tumor immune microenvironment (TIME).¹ A comprehensive examination of the tumor resident immune landscape, both pre- and post-immunotherapeutic interventions, has yielded insights into underlying factors contributing to the unresponsiveness of certain cancer types to immunotherapies.² This increasing understanding of the TIME holds immense promise for advancing the frontiers of solid tumor immunity.

Solid tumor types such as breast cancer (BC) and renal cell carcinoma (RCC) exhibit distinct TIMEs that influence their responses to immunotherapies. BC often develops an immunosuppressive tumor microenvironment characterized by elevated levels of regulatory T cells and myeloid-derived suppressor cells,^{3,4} which can reduce the effectiveness of immune checkpoint inhibitors like programmed cell-death 1 and its ligand (PD-1/PD-L1).⁵ In contrast, RCC is typically more immunogenic and responds better to these therapies.⁴ To enhance the immunogenicity of solid tumors, strategies targeting immunosuppressive innate immune cells, such as tumor-associated macrophages, are gaining significant attention.⁶ Another promising approach involves directly

CONTACT Juha Klefström  Juha.Klefstrom@helsinki.fi  Cancer Cell Circuitry Laboratory, Translational Cancer Medicine, Medical Faculty, University of Helsinki, Haartmaninkatu 8, 00290, Finland

*equal contribution.

**equal contribution, senior authors.

 Supplemental data for this article can be accessed online at <https://doi.org/10.1080/2162402X.2025.2466305>

© 2025 The Author(s). Published with license by Taylor & Francis Group, LLC.

This is an Open Access article distributed under the terms of the Creative Commons Attribution-NonCommercial License (<http://creativecommons.org/licenses/by-nc/4.0/>), which permits unrestricted non-commercial use, distribution, and reproduction in any medium, provided the original work is properly cited. The terms on which this article has been published allow the posting of the Accepted Manuscript in a repository by the author(s) or with their consent.

stimulating antigen-presenting cells (APCs) to prime CD8+ T cells for targeting tumor antigens, ultimately promoting both localized and systemic antitumor responses. One example is the direct activation of the stimulator of interferon genes (STING) pathway in APCs, which induces type I interferons and proinflammatory cytokines.^{7,8} The success of immunotherapy relies on the intricate and variable nature of the TIME, underscoring the necessity of evaluating it to guide personalized treatment selection and effectively stratify patients.

Several patient-derived *ex vivo* models have been developed in pursuit of uncovering resident immune cell interactions within the TIME.^{2,9–11} However, uncertainty remains regarding the optimization of *ex vivo* models for immuno-oncology research. On one hand, it is crucial to mimic the natural tumor tissue characteristics to understand interactions that occur under physiological conditions and tumor architecture.¹² However, creating more physiological models embedded in stiff materials and microfluidics devices, for example, may be prohibitively costly, or limit downstream applications. On the other hand, disregarding physiological conditions may induce artificial results and unwanted effects like immune cell efflux in the absence of added extracellular matrix.

To investigate how various culture techniques influence the response of resident immune cells to immunomodulation, we developed distinct *ex vivo* patient-derived explant culture (PDEC) models of breast cancer (BC) and renal cell carcinoma (RCC) independently in three different research groups. These models of breast and renal cell cancer-associated TIME represented increasing layers of processing defined as the manipulation of original tumor architecture and the addition of chemical cues. We used gene expression profiling and cytokine analyses to dissect the responses of immunotherapies targeting adaptive and innate immune cells. Our study demonstrates consistent patterns of immune activation across diverse *ex vivo* models of the TIME, revealing shared core signatures of adaptive and innate responses to immunomodulatory drugs, irrespective of the specific model or cancer type.

Materials and methods

Isolation of biological material and patient-derived models

PDEC “BC1” minimal manipulation; intact tissue architecture
Tumor tissue samples were collected in RPMI medium (Gibco) from treatment-naïve patients with breast cancer undergoing mastectomy surgery at the Turku University Hospital from Jan 2021 to Aug 2021. Written informed consent was obtained from each participant and the study was conducted under the approval of The Ethics Committee of the Hospital District of Southwest Finland (decision number: ETMK 132/2016) and in accordance with the ethical principles of the declaration of Helsinki.

Fresh tumor tissues were cut into small pieces with a scalpel to a diameter of <2 mm and frozen in RPMI (Sigma, cat. R5886) + 10% FCS + 1% GlutaMAX + penicillin-streptomycin (P/S, 12.8 U/mL, Gibco, cat.15140–122) supplemented with 10% DMSO at –150°C. The frozen tissue pieces were thawed

in a 37°C water bath and pelleted by centrifugation at 300g for 10 min at 10°C. The pieces were further cut (\approx 1.5 mm) and transferred on a 96-well low-attachment plate (Corning, cat.7007) for *ex vivo* treatment. The treatments were performed in quadruplicates in 200 μ L of RPMI + 10% FCS + 1% GlutaMAX + P/S and three tissue pieces per well.

PDEC “BC2” moderate manipulation; partial dissociation and embedding

Fresh tissue was obtained from the treatment-naïve elective breast cancer surgeries performed at the Helsinki University Central Hospital from 2020–2023 (Ethical permit: 243/13/03/02/2013/TMK02 157 and HUS/2697/2019 approved by the Helsinki University Hospital Ethical Committee), and in accordance with the ethical principles of the declaration of Helsinki. Patients participated in the study by signing a written informed consent form. As previously reported,¹¹ explants were made by incubating fresh primary tumor tissue overnight in collagenase A (3 mg/mL; Sigma) in MammoCult media (StemCell technologies) supplemented with mammo-cult proliferation supplement (StemCell technologies) with gentle shaking (130 rpm) at 37°C. The resulting tissue fragments were washed once with 1 \times PBS by centrifugation at 353g for 5 min. The fragments were resuspended in Cultrex Reduced Growth Factor Basement Membrane Extract, Type 2 (R&D Systems), and 37.5 μ L of matrix/fragment mixture was pipetted in the center of each well of an 8-chamber slide (Thermo Scientific). After matrix solidification (30 min), 500 μ L of supplemented MammoCult media was pipetted on top of each well.

PDEC “RCC” high manipulation; single cell dissociation, embedding, and media supplementation

Renal cell carcinoma tumor tissue was obtained from treatment-naïve patients undergoing radical or partial nephrectomy at the HUS Helsinki University Hospital. Studies were approved by the Helsinki University Hospital Ethical Committee (Dnro 115/13/03/02/15) and in accordance with the ethical principles of the declaration of Helsinki. Samples were obtained upon written informed consent. Tissues were preserved in MACS[®] tissue storage solution during transportation to the laboratory. Upon arrival, tumor tissue was dissociated using Miltenyi’s Tumor Dissociation kit (Miltenyi Biotec), and dissociated cells were live-frozen in 10% DMSO-FBS and stored at –150°C until use. Frozen tumor dissociates were thawed in AIM-V media, resuspended in Cultrex 3D Culture Matrix BME (Trevigen), and 35 μ L of matrix/cell suspension per treatment was applied on 8-well chamber slides (Lab-Tek). Following matrix solidification (20 min, +37 degrees), 400 μ L of AIM-V media supplemented with recombinant FGF (100 ng/mL), EGF (50 ng/mL), IL-2 (60 IU/mL), sodium pyruvate (10 mm), B-27 (1.5%), and r-spondin (50 ng/mL) was pipetted on top.

Drug treatments

Before experimentation, all drugs were aliquoted and distributed to ensure that each research group had access to the exact same lots. Each drug was aliquoted to minimize freezing/

thawing cycles. The explants were either left untreated or treated with 25 $\mu\text{L}/\text{mL}$ Immunocult (Stemcell, cat.10970), 10 μM ADU-S100 (MedChemExpress, cat. HY-12885), 50 $\mu\text{g}/\text{mL}$ pembrolizumab (MedChemExpress, cat. HY-P9902A), 10 $\mu\text{g}/\text{mL}$ magrolimab (Icosagen, clone 5F9) or 50 $\mu\text{g}/\text{mL}$ pembrolizumab and 10 $\mu\text{g}/\text{mL}$ magrolimab (combo). Drugs were added to the explant cultures immediately upon processing. After 48 h of *ex vivo* treatment at 37°C and 5% CO₂, cell culture supernatants were collected into fresh tubes and frozen at -70°C until analysis, while tissue fragments and cells were collected as described below in “nanostring gene expression profiling.”

Nanostring gene expression profiling

BC1 tissue pieces from replicate wells were collected in 1 mL of TRIsure (BioLine, cat. BIO-38032) and homogenized in gentleMACS M tubes (Miltenyi Biotec, cat. 130-093-236) using gentleMACS dissociator (Miltenyi Biotec, cat. 130-093-235) with program RNA.01_01. RNA was extracted according to the manufacturer’s protocol for TRIsure. Shortly, the samples were mixed with 200 μL chloroform and centrifuged at 12’000g for 15 min at 4°C. The aqueous phase containing the RNA was collected and precipitated with 500 μL cold isopropyl alcohol for 10 min at RT, and samples were centrifuged at 12’000g for 10 min at 4°C. Pellets were washed once with 1 mL 75% ethanol, air-dried, and dissolved in nuclease-free water (Ambion, cat. AM9930).

For BC2 and RCC, samples were centrifuged at 300–353g for 5 min to aspirate the remaining supernatant. The resulting tissue/cell pellets were extracted and total RNA was isolated using RNeasy (Qiagen) according to manufacturer instructions. BC1, BC2, and RCC model DNase removal and RNA concentration were performed using a commercial kit (Zymo Research, cat. R1013) according to the manufacturer’s instructions.

All samples went through QC (Qubit) (BC1 RIN 5.0–9.0; BC2 RIN 5.5–8.2; RCC RIN 6.4–9.5) before gene expression analysis on the NanoString nCounter gene expression platform (NanoString Technologies). nCounter Human PanCancer Immune Profiling Panel consisting of 770 genes to identify different immune cell types and their abundance, checkpoint molecules, cancer-testis (CT) antigens, and genes covering both the adaptive and innate immunological function. Per sample, 50 ng of total RNA in a final volume of 5 μL was mixed with a reporter code-set, hybridization buffer, and capture codeset. Samples were hybridized overnight at 65°C for 20 hours. Hybridized samples were run on the NanoString nCounter SPRINT profiler.

NanoString gene expression profiling results were analyzed using the nSolver advanced analysis software. During the normalization step, the housekeeping genes with AvgCount of less than 100 were removed. Differential expression analysis expression was performed with the Patient_id as a confounding factor.

P-values were adjusted by the Benjamini & Yekutieli method.¹³ Venn diagrams show differentially expressed genes that are statistically significant with a P-value of less than 0.05. Pathway scores are calculated as the first principal component of the pathway genes’ normalized expression. Pathway scores were adjusted with Patient_id as a confounding factor.

Pearson correlation between the estimated cell abundance in the untreated samples and the fold-change in immune activity pathways (treated/untreated) was calculated.

Cytokine profiling

Cytokine secretion was analyzed from cleared PDEC culture supernatants using Bio-Plex Pro Human Cytokine 27-plex assay kit (Bio-Rad, cat. M500KCAF0Y) and Bio-Plex 200 System (Bio-Rad) according to the manufacturer’s instructions. Results analyzed using Bio-Plex Manager 6.0 software (Bio-Rad Laboratories). Cytokines with > 10% of data points outside the detection range were excluded from the analyses. The remaining values lower than the detection limit were replaced by 0.5 ’ lowest measured value. Cytokines were visualized using GraphPad Prism (v.9.5.1). To identify changes in cytokine secretion following treatment, log₂FoldChanges were calculated.

Results

Ex vivo TIME landscape of breast cancer and renal cell carcinoma

To see how culturing conditions affect *ex vivo* immunotherapy responses, we compared three established patient-derived *ex vivo* models in increasing levels of manipulation (Figure 1a). The breast cancer model “BC1” represents the least disruptive system as it has very little hands-on processing, and the tumor architecture is mostly preserved. The breast cancer model “BC2”¹¹ is fragmented through mild enzymatic digestion, also resulting in intact tumor fragments with original tumor architecture.¹² BC2 fragments are further embedded into a 3D matrix, which provides structural support for several cell types. The renal cell carcinoma model “RCC” has the most amount of processing featuring enzymatic digestion of tumor material down to single cells, which are embedded in a 3D matrix and supplemented with IL-2 and growth factors.

In order to characterize the immunotherapy responses, the baseline immune cell composition and cytokine secretion profiles of the three model systems were assessed. Based on estimated cell abundances through gene expression profiling, the baseline immune cell composition differed across the three models, with RCC being richer in all immune cell types except mast cells and B cells in comparison to the BC models (Figure 1b). This is in line with a reported RNA-based pan-cancer analysis of 33 cancer types, which shows that RCC has more immune infiltrate and is considered more inflammatory.⁴ Between the two BC models, BC2 had higher estimated immune cell abundances (Figure 1b). Normalizing the immune cell abundances to the amount of tumor-infiltrating leukocytes

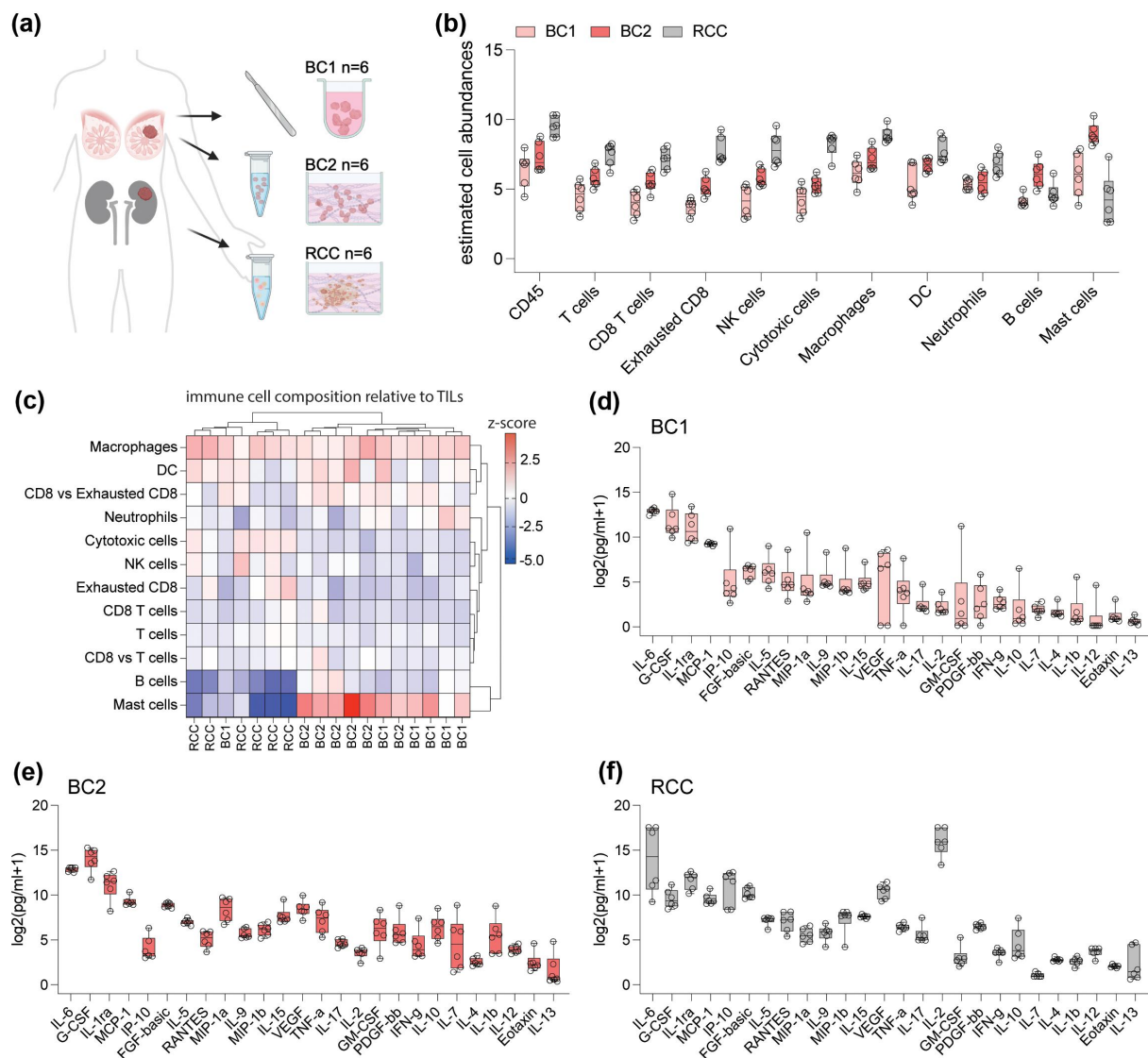


Figure 1. *Ex vivo* tumor landscape of breast cancer and renal cell carcinoma. a, Schematic representation of the processing of the patient-derived explant models, $n=6$ for each model, 'BC1', 'BC2' and 'RCC'. b, Comparison of the estimated cell type abundances (mean \pm SD) based on gene expression profiling 'BC1' = light pink, 'BC2' = dark pink and 'RCC' = grey. Cell abundance score refers to mean log₂ normalized counts of cell type specific markers. c, Estimated cell type score per patient normalized to tumor immune infiltration, depicting relative immune cell composition for each patient. Samples clustered with Ward's minimum variance method. Scale is z-score. d-f, Box and whisker (min to max) plot of baseline cytokine secretion of each patient presented as log₂ of the raw pg/ml (+1 as a small constant value).

revealed that BC1, BC2, and RCC samples had comparable macrophage infiltration, but the BC models had higher relative proportions of B cells and mast cells, and a lower relative proportion of cytotoxic cells (Figure 1c). Baseline cytokine profiling showed that all models were largely secreting similar chemokine profiles, including G-CSF, MCP-1 (CCL2), IP-10 (CXCL10), RANTES (CCL5) and MIP-1a/b (CCL3/4) (Figure 1d-f). This is in line with the high myeloid and lymphoid immune cell infiltration within the tumor models (Figure 1b),¹¹ and consistent with chemokines associated with these tumor types. Cell numbers were not calculated prior to culturing because that would have required the dissociation of the tumor fragments, therefore, we assessed cytokine relationships to each other rather than cytokine amounts across the models. The pleiotropic cytokine IL-6 was the most secreted cytokine in the TIME of each model (Figure 1d-f). IL-6 may be secreted by various immune cell types as well as

cancer cells, and its overexpression is reported ubiquitously in many cancer types.^{14,15} High levels of other pro-inflammatory cytokines, such as TNF- α , and interleukins with T-cell and NK-cell stimulatory properties (eg. IL-15) were also present in each model. As expected, RCC samples which consist of a highly vascularized tumor type¹⁶ showed proportionally increased vascular endothelial growth factor (VEGF) secretion in relation to cytokines that were expressed at similar levels in BC, like IL-15 (Figure 1d-f). Furthermore, we detected higher IL-2 levels in RCC as a result of IL-2 media supplementation (Figure 1f). When comparing the cytokine trends in BC1 and BC2 in comparison to a reference cytokine IP-10, BC2 had an increased trend toward higher baseline secretion of a T helper 2 type cytokines (IL-10, IL-4, IL-13), proinflammatory cytokines (IL-17, IFN- γ , IL-12, IL-1b), and growth factors and regulators (GM-CSF, IL-7, IL-2), possibly reflecting distinct immune landscape and composition in BC2

cultures. Similarly, G-CSF was generally expressed higher in BC than RCC (Figure 1d–f), perhaps due to the higher relative abundance of neutrophils and mast cells in BC (Figure 1c).

Importantly, while patient cytokine profiles were generally consistent for each model and cancer type, *ex vivo* modeling did not mask patient-specific variation (S1A–C). For example, “BC1” patient H72 with a clinical diagnosis of triple-negative breast cancer (TNBC) (S1D) displayed higher baseline secretion of cytokines like GM-CSF and G-CSF (S1A) compared to patients of the same model, consistent with previously published findings of high G-CSF secretion by TNBC cells compared to cells of other breast cancer types.¹⁷ Therefore, we found that the baseline immune contexture of each model was concordant with literature for these cancer types, and consistent across models (BC1 vs BC2) supporting further exploration of differences in immune response.

Effects of adaptive and innate immune modulation on immune cell abundance and cytokine secretion

To measure immunotherapy responses in our *ex vivo* models, we selected adaptive and innate immunomodulatory drugs with diverse mechanisms of action, clinical relevance, promising early-phase data, and prioritized one innate and one adaptive drug with maximal immune activation as benchmarks (Figure 2a). Anti-PD-1 (pembrolizumab) was included because it shows efficacy in RCC,^{18–21} and in TNBC in combination with chemotherapy^{22,23} despite limited application in other breast cancer subtypes. Magrolimab is a first-in-class humanized monoclonal CD47-binding antibody that prevents tumor cells from escaping macrophage phagocytosis, and is being tested in BC in combination with standard therapies (NCT04958785, NCT05807126). CD47 is also highly expressed in RCC patients and has been suggested as a candidate for anti-CD47 blockade.²⁴ Additionally, HX009, a PD1/CD47 bispecific mAb is under phase II clinical trial in solid tumors (NCT04886271), further prompting investigation of pembrolizumab and magrolimab alone and in combination in our models. To achieve maximal immune modulation, we also included non-clinical T-cell-activating Immunocult (anti-CD3/CD28/CD2), and the cyclic GMP-AMP synthase (cGAS)/stimulator of interferon genes (STING) pathway agonist (ADU-S100) to induce robust adaptive and innate immune activation, respectively.

Other drug candidates for the study included anti-HER2 (trastuzumab), anti-EGFR (cetuximab), as well as positive controls lipopolysaccharide (LPS) and a cocktail of IL-2/IL-15 (S2, S3). The final drug panel was narrowed down to 6 conditions based on clinical relevance and/or benchmark signal intensity to ensure all samples from one patient fit on the same nanostring cartridge to prevent differences due to batch effects. Positive control compounds like LPS and IL-2/IL-15 were removed from the limited final panel as they were mainly included to optimize the readout and timepoints. Selecting drug candidates with adequately robust adaptive or innate inflammatory signal induction (Immunocult; ADUS100) ensured that there was a strong enough response to compare

across all three models. Pilot gene expression profiling ($n = 1$ per treatment) revealed that Immunocult, ADU-S100, LPS and anti-CD47 evoked a stronger response at 48hrs compared to 24hrs (S2A), prompting the selection of the 48 hr timepoint. The remaining treatments showed little effect (S2). Similarly, cytokine profiling of the same samples showed a modest response to anti-PD-1, anti-EGFR, anti-HER2, and IL-2/IL-12 supplementation, although some immune activation was observed, evident by the induction of IP-10 (S3A–H).

Thus, BC1, BC2 and RCC were treated with the panel of drugs (Figure 2a) for 48 hrs, and 6 out of 8 patient samples for each model with the highest cytokine responses following treatment were further analyzed with gene expression profiling (S1A–C). First, we analyzed immune cell abundances following treatment to give context to the subsequent gene expression pathway and cytokine analyses. The estimated CD45+ leukocyte abundances were mostly unaffected, aside from a statistically significant decrease in total leukocytes in BC2 following ADU-S100 (Figure 2b). The leukocytes that were depleted in BC2 following ADU-S100 likely represent a combination of cell types that are slightly depleted following treatment, but not significantly as individual cell types. Examples would include T cells and B cells, which are slightly decreased in BC2 (S4A–B). A similar trend was not seen in the other BC model, nor with RCC embedded in the same matrix, suggesting there may be additional cytokines in BC1 and RCC which may support T cells and B cells following STING-agonism. T cells, CD8+ T cells, B cells, DCs, and mast cells did not change in numbers following immunomodulation with any of the tested compounds (Figure 2c–d, S4A–D). However, T cell activation achieved with Immunocult did have a significant positive impact on the amount of NK cells (BC1, BC2, RCC), cytotoxic CD8+ T cells (BC1), and exhausted CD8 + T cells (BC1, RCC), and a significant negative effect on macrophages (RCC), and neutrophils (RCC) (Figure 2D–H). These findings are relevant for subsequent interpretation of pathway and cytokine analyses, where gene expression changes and cytokine secretion following treatments with sustained cell numbers are more likely biological responses than reflections of changing cell numbers.

Immunocult induced a robust effect on cytokine secretion in all models, however, the magnitude and the diversity of the response were strikingly different with model-specific log₂FC ranging from 2 (BC2) to 20 (BC1) (Figure 3a). Cytokines representing immune activation (IP-10, TNF- α) after T cell stimulation were following a similar trend, and detected across all three explant models. However, BC1 and RCC models additionally exhibited numerous statistically significant secretion of chemokines (eg. GM-CSF, MIP-1a/b, RANTES, eotaxin) and cytokines (eg. IL-12, IL-10, IL-17, IL-13). Individual patient samples from all models showed induction of T helper type I and type II cytokines (S5A–C). The STING agonist ADU-S100 triggered distinct activation patterns based on the unique thresholds of each model, leading to increased secretion of RANTES, MIP-1 α , MIP-1 β , and TNF- α (Figure 3a). The remaining compounds, pembrolizumab, magrolimab and their combination showed more modest and selective

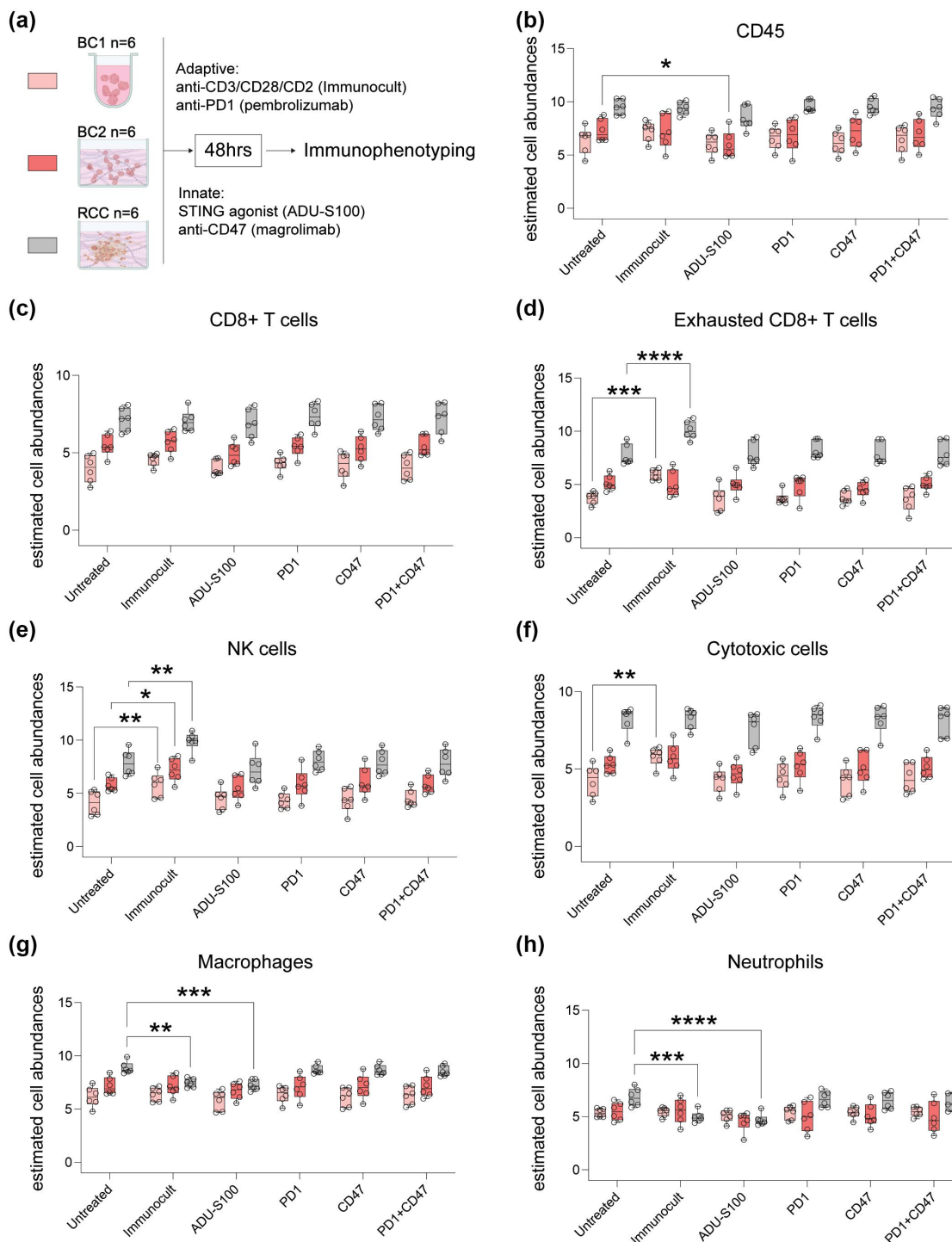


Figure 2. Effect of adaptive and innate immune modulation on cell abundances. a, Schematic of treatments selected for the study b, Box and whisker (min to max) of total estimated cell abundances after immunomodulation. c, No significant changes in CD8+ T cell numbers, but significant changes in d, exhausted CD8+ T cells e, NK cells f, cytotoxic cells g, macrophages, and h, neutrophils. Statistical significance was tested with a two-way ANOVA with Fishers LSD. All data are presented as mean values \pm SD. ($p = **** = <0.0001$; $p = *** = <0.001$; $p = ** = <0.01$; $p = * = <0.05$).

stimulation in comparison to Immunocult and STING-agonism in each model, revealing more patient-specific stimulation (S5A-C). Notably, IL-2-supplemented RCC showed a significant drop in IL-2 levels following Immunocult treatment (Figure 3a).

In summary, the tumor immune cell abundances and cytokine secretion profiles demonstrated consistent qualitative responses to immune modulation across models, even though the intensity of the responses varied significantly.

PDECs reflect biological changes in response to immunomodulation

We further confirmed the activation of immune-related pathways using transcriptional profiling with Nanostring (Figure 3b, S6A-D). As observed with the secreted cytokines, Immunocult led to robust T cell activation in each model, stimulating chemokine, cytokine, and interleukin pathways. As with the cytokines, the magnitude of this response can be

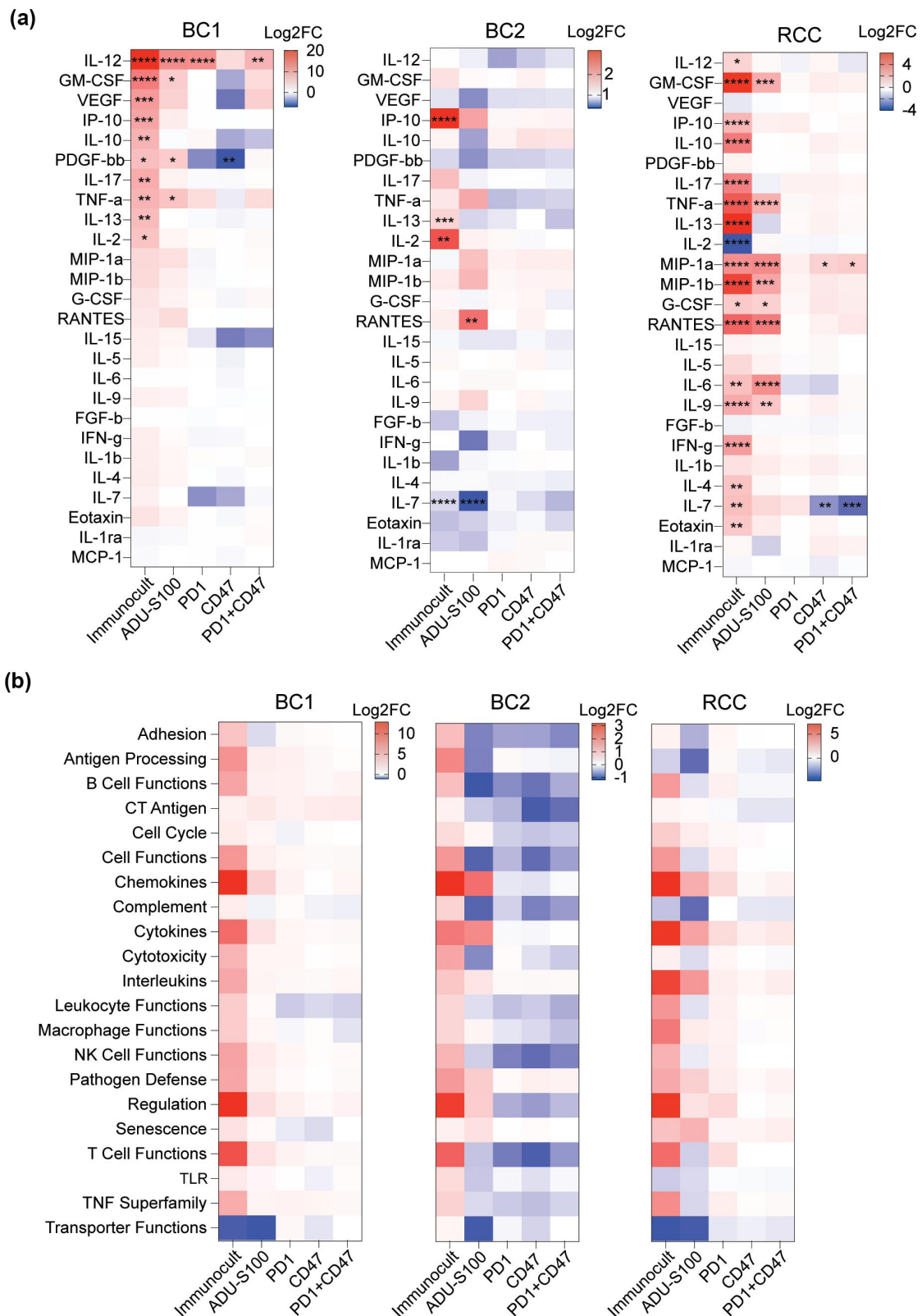


Figure 3. *Ex vivo* cultures reflect biological changes in response to immunomodulation. a. BC1, BC2 and RCC cytokine responses of each treatment shown as log₂FC (treated explants to untreated controls). Statistical significance was tested with a two-way ANOVA with Fishers LSD. ($p = **** = <0.0001$; $p = *** = <0.001$; $p = ** = <0.01$; $p = * = <0.05$) b, heatmap of average BC1, BC2 and RCC patient pathway score determined by gene expression profiling. The scale reflects the treated pathway score – the untreated pathway score.

interpreted as the maximum T cell activation threshold for that specific model, and can be used as a reference when testing whether patients have the ability to respond to immunomodulation (S6A). The STING-agonist ADU-S100 also showed a strong response, although more restricted to expected pathways (eg. chemokines) in innate immune modulation (Figure 3b). The RCC samples presented the most notable response to PD-1 blockade, which resembled Immunocult responses albeit at a lower stimulation magnitude. This was accompanied by an increase in various cell functions (B-, NK- and T-cell, leukocyte, and macrophage functions) as well as stimulation of interleukin, cytokine, and chemokine pathways (Figure 3b). These effects were more modest in the BC models (Figure 3b). However, without clinical response data to anti-PD-1, it is not clear whether the addition of IL-2 in the RCC culture medium primed anti-PD-1 resistant tumor samples to ICB, as seen in *ex vivo* melanoma cultures with low baseline secretion of IL-2,²⁵ or whether the higher response in comparison to BC is because RCC is generally more sensitive to anti-PD-1 therapy.

We next explored the possibility that tumor properties correlate with *ex vivo* treatment responses. We analyzed the correlation of baseline immune cell abundance with treatment response (S7A-E). For instance, baseline T-cell abundance did not influence the magnitude of the increase in ‘T cell functions’ following treatments aiming at T-cell activation (S7A). Meanwhile, the number of DCs at baseline seemed to closely correlate with macrophage functions following T cell activation, STING agonism, and treatment with anti-PD-1 (S7B). Other studies have shown that major physiological functions of type I interferons are directed toward DCs,²⁶ making it plausible that DC numbers correlate with treatment response.

Core innate and adaptive immune response signatures as potential biomarkers

As BC and RCC *ex vivo* models generally responded similarly to immunomodulation, we pooled the Nanostring gene expression analyses from all samples together and generated a core response signature for T cell activation (adaptive, Immunocult) and interferon signaling (innate, ADU-S100). Among the different treatment approaches, Immunocult induced the highest number of differentially expressed genes (Figure 4a), and this was more robustly seen in BC1 and RCC models. Interestingly, the three PDEC models generated a shared upregulated ‘core response’ gene set for Immunocult: *CCL2*, *CCL7*, *CCL8*, *CD274*, *CFB*, *CX3CL1*, *CXCL10*, *CXCL11*, *CXCL9*, *ICAM1*, *IDO1*, *IL15RA*, *IRF1*, *JAK2*, *SERPING1*, *SOCS1*, *TAP1*, *TAP2*, *XL2* (Figure 4b). The models did not share any downregulated genes following Immunocult treatment (Figure 4b). The pathways associated with the upregulated core response signature were analyzed in the Metascape²⁷ validating the responses to the activation of an adaptive immune response and more selectively to type 2 interferon signaling (Figure 4c). Then we tested our “Adaptive signature” of T cell activation using the Tumor Immune Dysfunction and Exclusion (TIDE) computational framework of post PD-1-treated melanoma patients, and found that our “Adaptive signature” was able to stratify

patients treated with anti-PD-1^{28–30} for better overall survival on par with existing biomarkers for immunotherapy including IFN γ , CD8+ infiltration, and a biomarker developed by Merck (Figure 4d–e).

Through a similar analysis, STING-agonism through ADU-S100 also induced robust but more modest gene expression changes than direct T cell activation, as determined by comparing the magnitude of the fold-change response (Figure 4f). The shared upregulated core genes for innate activation were: *BST2*, *CCL5*, *CXCL11*, *DDX58*, *IFI27*, *IFI35*, *IFIH1*, *IFIT1*, *IFIT2*, *IFITM1*, *IRF7*, *ISG15*, *ISG20*, *MIX1*, *NT5E*, *OAS3*, *STAT2* (Figure 4g). Interestingly, BC2 had more unique upregulated genes following ADU-S100 treatment, while BC1 had more upregulated genes following T cell activation (Figure 4b, g). Activating the STING pathway had an expected effect of downregulating CD14 which was seen in all three models (Figure 4g). Upregulated innate core genes were involved in type I interferon response and interferon alpha/beta signaling (Figure 4h). This signature was comparable in terms of predicting overall survival as the T cell signature, presumably reflecting the overall positive association of the baseline pro-inflammatory tumor immune microenvironment on ICB clinical response (Figure 4i–j). Individual genes were not significantly upregulated following pembrolizumab, magrolimab, or pembrolizumab + magrolimab treatments from pooled samples (S8A–C). Notably, genes (*CMKLR1*, *CCL18*, *IL6R*) within the NF- κ B-IL6 pathway were downregulated only with the combination of pembrolizumab + magrolimab, although not significantly.

Discussion

Human *ex vivo* tumor models have been used to dissect early immunotherapy responses^{2,9,10} with promising predictive potential for patients receiving immune-checkpoint blockade (ICB) therapy.² However, the development of human-derived *ex vivo* models is not standardized, and it is unclear how the disruption of the tissue architecture and *ex vivo* culture conditions influence immunotherapy responses. We compared immunotherapy responses across three independently developed *ex vivo* patient-derived explant systems. Our findings demonstrated that while the magnitude of the response varied between model systems, the qualitative nature of the responses was remarkably consistent, revealing shared signatures of adaptive and innate immune activation.

This shared qualitative nature was unexpected, given the numerous variables in the data – patient heterogeneity, two cancer types with multiple subtypes, and three culturing conditions. Direct head-to-head comparisons of treatment responses using the same material across three distinct models were not feasible due to limited tissue availability, constrained by the tumor size received in the lab. Nevertheless, common responses were especially surprising given possible changes in the immune composition, such as a potential immune efflux in the BC1 model in the absence of matrix embedding, as evidenced by lower CD45 infiltration, or potential benefits of the extracellular matrix (ECM) for maintaining cell types like dendritic cells (DCs).³¹ These ECM-driven effects could explain why BC2 exhibited more pronounced gene expression changes following

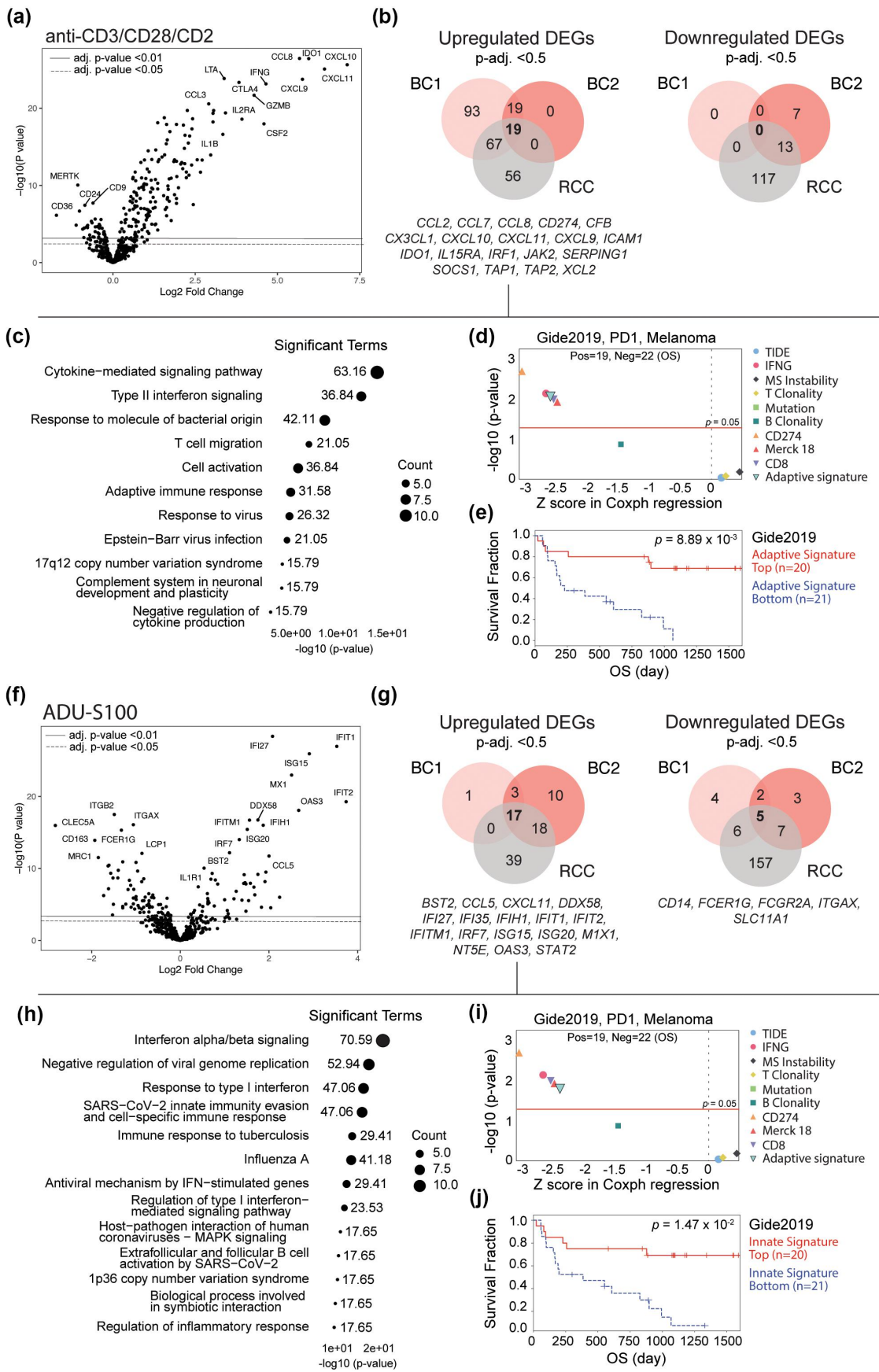


Figure 4. Core innate and adaptive response signatures as potential biomarkers. a, Differentially expressed genes of pooled explant samples following Immunocult treatment. Genes above the solid line are adjusted p-value < 0.01, genes above dotted line are adjusted p-value < 0.05. b, Venn diagram of significantly (adjusted p-value < 0.5) upregulated genes following Immunocult, shared core gene signature of 19 genes is bolded, and core genes are listed below the plot, and Venn diagram of significantly downregulated genes following Immunocult. c, Metascape analysis of pathways associated with the core signature, circle size refers to the number of core genes (=count) matching the pathway, and the numerical value is the percentage of all of the user-provided genes that are found in the given ontology term. *Log10

innate activation. The ability of the core response signatures to predict PD-1 responses is less surprising, as high IFN- γ signatures have been shown to correlate with PD-1 responsiveness,³² highlighting the consistencies of *ex vivo* observations with existing clinical literature. We believe that the shared signatures are partly due to short-term culturing, where the limited duration minimizes the impact of the culture method on the phenotype of immune and cancer cells.^{11,12} Over time, as certain immune cell subsets are lost and cancer cells adapt to the new microenvironment, a common response may become less likely. Additionally, *ex vivo* explants may reveal treatment responses that are difficult to capture *in vivo*, where drug penetration into solid tumors can be a limiting factor. By preserving the native tumor-immune microenvironment, we suggest that short-term explant cultures provide a robust platform for investigating TIME responses in immuno-oncology, despite technical variations and tumor type differences.

Mechanistically, patient-derived *ex vivo* cultures provide valuable insights into the pathways altered in tumor-resident immune cells following treatment, even when the primary target of the therapy is not the immune system.¹¹ The combination of pembrolizumab and magrolimab uniquely, but not significantly, downregulated genes within the NF- κ B-IL6 pathway, an effect not observed with either drug alone. Although the sample size and experimental setup do not support detailed mechanistic conclusions, this observed synergy warrants further investigation. Previous *in vitro* studies suggest that targeting this pathway in cancer-associated fibroblasts in breast cancer could normalize the tumor stroma, potentially enhancing anti-cancer effects.³³

Statistically, patient-derived *ex vivo* models present unique challenges, particularly due to the influence of culture conditions on the maximum response threshold. For instance, the BC2 model consistently demonstrated modest changes in cytokine secretion and gene expression, even at peak levels, compared to other models. This relatively limited variability between min and max makes it unreasonable to compare responses between methods using the same statistical assumptions. Instead, robust empirical methods like the Boolean implication network that takes into account the qualitative relationships between genes rather than the p-value, may become the benchmark for comparing future *ex vivo* studies.³⁴ Nevertheless, as all findings will ultimately be validated using alternative methods, we argue that subtle but consistent responses should not be prematurely dismissed due to a lack of statistical significance, especially when they align with expected mechanistic pathways. The next step involves leveraging these results to build on established clinical benchmarks, where larger-scale validation and clinical data can provide a more precise interpretation of their biological relevance.

In summary, our study presents immunotherapy treatment responses across three independent *ex vivo* models of breast cancer and renal cell carcinoma. We observed robust activation of both adaptive and innate immune responses, leading to the identification of two shared core immune signatures – adaptive and innate – that could serve as potential exploratory biomarkers for predicting treatment outcomes. This work not only reveals several consistencies between *ex vivo* observations and previously published clinical data but also highlights the value of patient-derived *ex vivo* models in uncovering immune mechanisms. Such insights could inform future research aimed at improving patient stratification and optimizing therapeutic strategies.

Acknowledgments

We thank the study participants, the study nurses, the investigators, and the research team who contributed to the study. We also want to thank Mari Parsama and Teija Kanasuo technical assistance. Nanostring analysis was carried out at the functional genomics unit (FuGU) at the University of Helsinki.

Disclosure statement

No potential conflict of interest was reported by the author(s).

Funding

The present works were mainly funded through the Business Finland Health program award for project Cancer IO. Klefström research group has received funding from the Academy of Finland, Business Finland, the Finnish Cancer Organizations, Sigrid Jusélius foundation, Jane and Aatos Erkkö foundation, the Research Council of Finland, and RESCUER project, which has received funding from the European Union's Horizon 2020 Framework Programme (no. 847912). This work was also supported by the U.S. Department of Defense for Health Affairs through the Breast Cancer Research Program [award no. W81XWH2110773]. Opinions, interpretations, conclusions, and recommendations are those of the author and are not necessarily endorsed by the Department of Defense. In addition, funds were received from Sihtasutus Archimedes, Ida Montinin Säätiö, Finnish Cancer Institute, Syöpäjärjestöt, and the iCAN Digital Precision Cancer Medicine Flagship. Mustjoki research group has received funding from Cancer Foundation Finland, Academy of Finland, Sigrid Jusélius Foundation, Gyllenberg Foundation, Jane and Aatos Erkkö Foundation, State funding for the University-level Health Research in Finland, and HiLIFE fellow funds. Hollmén research group has received funding from Academy of Finland, Cancer Foundations, and the Sigrid Jusélius Foundation.

ORCID

Juha Klefström  <http://orcid.org/0000-0001-7124-8431>

(P) is the p-value in log base 10. d, the core "Adaptive signature" in relation to existing biomarkers for immunotherapies in a cohort of anti-PD-1 treated melanoma patients from Gide et al., 2018 e, overall survival of anti-PD-1-treated melanoma patients with higher (red) vs. lower (blue) core adaptive core signature expression. f, Differentially expressed genes of pooled explant samples following ADU-S100 treatment g, venn diagram of significantly upregulated genes following ADU-S100, and core genes are listed below the plot, and venn diagram of significantly downregulated genes following ADU-S100 h, Metascape analysis of pathways associated with the core signature, circle size refers to the amount of core genes matching the pathway, and the numerical value is the percentage of all of the user-provided genes that are found in the given ontology term. "Log10(P)" is the p-value in log base 10. i, the adaptive core "innate signature" in relation to existing biomarkers for immunotherapies in a set of anti-PD-1 treated melanoma patients j, overall survival of anti-PD-1-treated melanoma patients with higher (red) vs. lower than median core innate signature expression (blue) of the core innate signature. OS, overall survival.

Author contributions

R.T., A.T., J.P., M.H., S.M., and J.K., designed the study; R.T, K.P., J.H.R., R.L, and A.N.K optimized *ex vivo* cultures and treated explants, and collected data. R.T., K.P., J.H.R., and D.N analyzed and visualized the data. M.M., P.E.K., L.N., T.M., J.M., P.J., K.L., R.J., S.T., T.M., P.B., and I. K., recruited patients, and collected clinical data, R.T., K.P., M.H., S.M, and J.K interpreted the data, R.T, K.P., M.H., S.M., J.K., wrote the first draft of the manuscript. All authors reviewed the manuscript and approved the final version.

Data availability statement

The data that support the findings of this study are available from the corresponding author, JK, upon reasonable request.

References

- Najafi M, Goradel NH, Farhood B, Salehi E, Solhjoo S, Toolee H, Kharazinejad E, Mortezaee K. Tumor microenvironment: Interactions and therapy. *J Cellular Physiol.* 2019;234(5):5700–5721. doi:10.1002/jcp.27425.
- Voabil P, de Bruijn M, Roelofs LM, Hendriks SH, Brokamp S, van den Braber M, Broeks A, Sanders J, Herzig P, Zippelius A, et al. An *ex vivo* tumor fragment platform to dissect response to PD-1 blockade in cancer. *Nat Med.* 2021;27(7):1250–1261. doi:10.1038/s41591-021-01398-3.
- Soysal SD, Tzankov A, Muenst SE. Role of the tumor microenvironment in breast cancer. *Pathobiology.* 2015;82 Preprint at 3–4):142–152. doi:10.1159/000430499.
- Thorsson V, Gibbs DL, Brown SD, Wolf D, Bortone DS, Ou Yang T-H, Porta-Pardo E, Gao GF, Plaisier CL, Eddy JA, et al. The immune landscape of cancer. *Immunity.* 2018;48(4):812–830. e14. doi:10.1016/j.immuni.2018.03.023.
- De Visser KE, Joyce JA. The evolving tumor microenvironment: from cancer initiation to metastatic outgrowth. *Cancer Cell.* 2023;41 Preprint at 3):374–403. doi:10.1016/j.ccell.2023.02.016.
- Rannikko JH, Hollmén M. Clinical landscape of macrophage-reprogramming cancer immunotherapies. *Br J Cancer.* 2024;131(4):627–640. doi:10.1038/s41416-024-02715-6.
- Sivick KE, Desbien AL, Glickman LH, Reiner GL, Corrales L, Surh NH, Hudson TE, Vu UT, Francica BJ, Banda T, et al. Magnitude of therapeutic STING activation determines CD8+ T cell-mediated anti-tumor immunity. *Cell Rep.* 2018;25(11):3074–3085.e5. doi:10.1016/j.celrep.2018.11.047.
- Corrales L, Glickman L, McWhirter S, Kanne D, Sivick K, Katibah G, Woo S-R, Lemmens E, Banda T, Leong J, et al. Direct activation of STING in the tumor microenvironment leads to potent and systemic tumor regression and immunity. *Cell Rep.* 2015;11(7):1018–1030. doi:10.1016/j.celrep.2015.04.031.
- Yuki K, Cheng N, Nakano M, Kuo CJ. Organoid models of tumor immunology. *Trends Immunol.* 2020;41 Preprint at 8):652–664. doi:10.1016/j.it.2020.06.010.
- Jenkins RW, Aref AR, Lizotte PH, Ivanova E, Stinson S, Zhou CW, Bowden M, Deng J, Liu H, Miao D, et al. *Ex vivo* profiling of PD-1 blockade using organotypic tumor spheroids. *Cancer Discov.* 2018;8(2):196–215. doi:10.1158/2159-8290.CD-17-0833.
- Turpin R, Liu R, Munne PM, Peura A, Rannikko JH, Philips G, Boeckx B, Salmelin N, Hurskainen E, Suleymanova I, et al. Respiratory complex I regulates dendritic cell maturation in explant model of human tumor immune microenvironment. *J Immunother Cancer.* 2024;12(4):e008053. doi:10.1136/jitc-2023-008053.
- Munne PM, Martikainen L, Rätty I, Bertula KN, Ruuska J, Ala-Hongisto H, Peura A, Hollmann B, Euro L, et al. Compressive stress-mediated p38 activation required for ER α + phenotype in breast cancer. *Nat Commun.* 2021;12(1). doi:10.1038/s41467-021-27220-9.
- Benjamini Y, Hochberg Y. Controlling the false discovery rate: a practical and powerful approach to multiple testing. *J R Stat Soc Ser B: Stat Methodol.* 1995;57(1):289–300. doi:10.1111/j.2517-6161.1995.tb02031.x.
- Hunter CA, Jones SA. IL-6 as a keystone cytokine in health and disease. *Nat Immunol.* 2015;16 Preprint at 5):448–457. doi:10.1038/ni.3153.
- Guo Y, Xu F, Lu T, Duan Z, Zhang Z. Interleukin-6 signaling pathway in targeted therapy for cancer. *Cancer Treat Rev.* 2012;38 Preprint at 7):904–910. doi:10.1016/j.ctrv.2012.04.007.
- Mertz KD, Demichelis F, Kim R, Schraml P, Storz M, Diener P-A, Moch H, Rubin MA. Automated immunofluorescence analysis defines microvessel area as a prognostic parameter in clear cell renal cell cancer. *Hum Pathol.* 2007;38(10):1454–1462. doi:10.1016/j.humpath.2007.05.017.
- Hollmén M, Karaman S, Schwager S, Lisibach A, Christiansen AJ, Maksimow M, Varga Z, Jalkanen S, Detmar M. G-CSF regulates macrophage phenotype and associates with poor overall survival in human triple-negative breast cancer. *Oncoimmunology.* 2016;5(3):e1115177. doi:10.1080/2162402X.2015.1115177.
- Rini BI, Plimack ER, Stus V, Gafanov R, Hawkins R, Nosov D, Pouliot F, Alekseev B, Soulières D, Melichar B, et al. Pembrolizumab plus axitinib versus sunitinib for advanced renal-cell carcinoma. *N Engl J Med.* 2019;380(12):1116–1127. doi:10.1056/NEJMoa1816714.
- Choueiri TK, Tomczak P, Park SH, Venugopal B, Ferguson T, Chang Y-H, Hajek J, Symeonides SN, Lee JL, Sarwar N, et al. Adjuvant Pembrolizumab after Nephrectomy in Renal-Cell Carcinoma. *N Engl J Med.* 2021;385(8):683–694. doi:10.1056/NEJMoa2106391.
- Motzer RJ, Escudier B, McDermott DF, George S, Hammers HJ, Srinivas S, Tykodi SS, Sosman JA, Procopio G, Plimack ER, et al. Nivolumab versus everolimus in advanced renal-cell carcinoma. *N Engl J Med.* 2015;373(19):1803–1813. doi:10.1056/NEJMoa1510665.
- Xu JX, Maher VE, Zhang L, Tang S, Sridhara R, Ibrahim A, Kim G, Pazdur R. FDA approval summary: nivolumab in advanced renal cell carcinoma after anti-angiogenic therapy and exploratory predictive biomarker analysis. *Oncologist.* 2017;22(3):311–317. doi:10.1634/theoncologist.2016-0476.
- Rugo HS, Schmid P, Cescon DW, Nowecki Z, Im S-A, Yusof MM, Gallardo C, Lipatov O, Barrios CH, Perez-Garcia J, et al. Abstract GS3-01: additional efficacy endpoints from the phase 3 KEYNOTE-355 study of pembrolizumab plus chemotherapy vs placebo plus chemotherapy as first-line therapy for locally recurrent inoperable or metastatic triple-negative breast cancer. *Cancer Res.* 2021;81(4_Supplement):GS3-01–GS3-01. doi:10.1158/1538-7445.SABCS20-GS3-01.
- Cortés J, Cescon DW, Rugo HS, Im S-A, Md Yusof M, Gallardo C, Lipatov O, Barrios CH, Perez-Garcia J, Iwata H, et al. LBA16 KEYNOTE-355: final results from a randomized, double-blind phase III study of first-line pembrolizumab + chemotherapy vs placebo + chemotherapy for metastatic TNBC. *Ann Oncol.* 2021;32:S1289–S1290. doi:10.1016/j.annonc.2021.08.2089.
- Park HR, Kim S-E, Keam B, Chung H, Seok SH, Kim S, Kim M, Kim TM, Doh J, Kim D-W, et al. Blockade of CD47 enhances the antitumor effect of macrophages in renal cell carcinoma through trogocytosis. *Sci Rep.* 2022;12(1). doi:10.1038/s41598-022-16766-3.
- Kaptein P, Jacobberger-Foissac C, Dimitriadis P, Voabil P, de Bruijn M, Brokamp S, Reijers I, Versluis J, Nallan G, Triscott H, et al. Addition of interleukin-2 overcomes resistance to neoadjuvant CTLA4 and PD1 blockade in *ex vivo* patient tumors. *Sci Transl Med.* 2022;14(642). doi:10.1126/scitranslmed.abj9779.
- Diamond MS, Kinder M, Matsushita H, Mashayekhi M, Dunn GP, Archambault JM, Lee H, Arthur CD, White JM, Kalinke U, et al. Type I interferon is selectively required by dendritic cells for immune rejection of tumors. *J Exp Med.* 2011;208(10):1989–2003. doi:10.1084/jem.20101158.
- Zhou Y, Zhou B, Pache L, Chang M, Khodabakhshi AH, Tanaseichuk O, Benner C, Chanda SK. Metascape provides a

- biologist-oriented resource for the analysis of systems-level datasets. *Nat Commun.* 2019;10(1). doi:10.1038/s41467-019-09234-6.
28. Jiang P, Gu S, Pan D, Fu J, Sahu A, Hu X, Li Z, Traugh N, Bu X, Li B, et al. Signatures of T cell dysfunction and exclusion predict cancer immunotherapy response. *Nat Med.* 2018;24(10):1550–1558. doi:10.1038/s41591-018-0136-1.
 29. Fu J, Li K, Zhang W, Wan C, Zhang J, Jiang P, Liu XS. Large-scale public data reuse to model immunotherapy response and resistance. *Genome Med.* 2020;12(1). doi:10.1186/s13073-020-0721-z.
 30. Gide TN, Quek C, Menzies AM, Tasker AT, Shang P, Holst J, Madore J, Lim SY, Velickovic R, Wongchenko M, et al. Distinct immune cell populations define response to anti-PD-1 monotherapy and anti-PD-1/Anti-CTLA-4 combined therapy. *Cancer Cell.* 2019;35(2):238–255.e6. doi:10.1016/j.ccell.2019.01.003.
 31. Shankar SP. Dendritic cells and the extracellular matrix: a challenge for maintaining tolerance/homeostasis. *World J Immunol.* 2015;5(3):113. doi:10.5411/wji.v5.i3.113.
 32. Ayers M, Lunceford J, Nebozhyn M, Murphy E, Loboda A, Kaufman DR, Albright A, Cheng JD, Kang SP, Shankaran V, et al. IFN- γ -related mRNA profile predicts clinical response to PD-1 blockade. *J Clin Investigation.* 2017;127(8):2930–2940. doi:10.1172/JCI911190.
 33. Hendrayani SF, Al-Harbi B, Al-Ansari MM, Silva G, Aboussekhra A. The inflammatory/cancer-related IL-6/STAT3/NF- κ B positive feedback loop includes AUF1 and maintains the active state of breast myofibroblasts. *Oncotarget.* 2016;7(27):41974–41985. doi:10.18632/oncotarget.9633.
 34. Sahoo D, Dill DL, Gentles AJ, Tibshirani R, Plevritis SK. Boolean implication networks derived from large scale, whole genome microarray datasets. *Genome Biol.* 2008;9(10). doi:10.1186/gb-2008-9-10-r157.